Interferometric Laser imaging technique applied to nuclei size measurements in cavitation tunnel

L. Mees, Denis Lebrun, Didier Fréchou, Romuald Boucheron

Interferometric Laser imaging technique applied to nuclei size measurements in cavitation tunnel.

L. Méès[1], Denis Lebrun[2], Didier Fréchou[3] and Romuald Boucheron[3]

[1] LMFA – UMR CNRS 5509, Ecole centrale de Lyon, 69134 Ecully Cedex, France

[2] CORIA – UMR CNRS 6614, Université et INSA de Rouen, 76801 Saint-Etienne du Rouvray, France

[3] DGA, Techniques Hydrodynamiques, (formelly Bassin d'essai des carènes), 27100 Val-de-reuil, France

ABSTRACT

Interferometric Laser Imaging Technique (ILIT) is applied to nuclei size measurements in cavitation tunnel. The use of a large collection angle optics is needed to allow nuclei size measurement down to 10 µm at 1 m distance. The negative effect of spherical aberration in such a situation is exhibited. A lens assembly, free from spherical aberrations and specifically designed for this application is presented. Measurements in a cavitation tunnel shows nuclei size distributions in the range 10-200µm. In addition to bubble sizes, ILIT can provide information on bubble concentration. To do so, a measurement volume is defined from statistical information extracted from the ILIT results themselves.

INTRODUCTION

The operational requirements for naval and research vessels has seen an increasing demand for quieter ships. Hence, the management of a ship's hydrodynamic signature requires better and more reliable estimates of propeller noise. One of the major sources of radiated noise is the occurrence of cavitation on the ship propeller. This makes the cavitation inception prediction a critical issue to assess for propeller model scale testing in hydrodynamic tunnels.

The water quality or nuclei content control is essential in a hydrodynamic tunnel dedicated to cavitation studies. Several studies [1,2] have confirmed the merit of the nuclei control for cavitation tests. Most of the cavitation tunnels control the nuclei content indirectly by controlling the dissolved air content of the water. The water quality usually varies with time and tests sequences. The French large cavitation tunnel is one of the rare facilities in which the nuclei content is controlled through micro-bubbles injection [3,4] independently of the dissolved air content control. Other tunnels like AMC in Australia, LEGI in Grenoble France and pump or turbine loops use the same technique. This method guarantees the repeatability of the test conditions over time.

The nuclei content measurement is required to ensure that the critical pressure of the water is close to the vapor pressure and to know the density of active nuclei. This implies the measurement of bubbles sizes in the typical range 20µm - 100µm. The Interferometric Laser Imaging Technique (ILIT) has been largely developed for droplets sizing, mainly because there are more industrial applications with droplets than with micro-bubbles. The technique is then often called ILIDS for Interferometric Laser imaging Droplet Sizing. But the ILIT principle remains valid for any transparent particles with quasi-spherical shape (or circular section).

ILIT PRINCIPLE

The ILIT technique uses a laser sheet that illuminates the particles in the flow and a camera that records images of particles passing through the Laser sheet. This technique has been first demonstrated for isolated droplets by Ragucci [5] but it has been applied to a droplet spray, showing its real potential, by Glover *et al* [6]. The scattered diagram (intensity versus scattering angle) of a transparent spherical particle shows oscillations. These oscillations are due to interferences between diffracted, reflected light and refracted light. In case of droplets and in the forward scattering region between 20° and 70° (standard ILIDS configuration [6]), these oscillations are mainly produced by interference between reflection and first order refraction. The fringe's angular frequency depends on the droplet size (interferometric sizing principle). In the case of bubbles, at a scattered angle around 90° between the laser propagation direction and the observation direction, fringes are mainly produced by interferences between refection and second order refraction (see fig. 1). In any case, the fringe pattern produced around a given angle can be calculated by using Lorenz-Mie Theory (LMT) to establish a relation between the fringe frequency and the particle size [7].

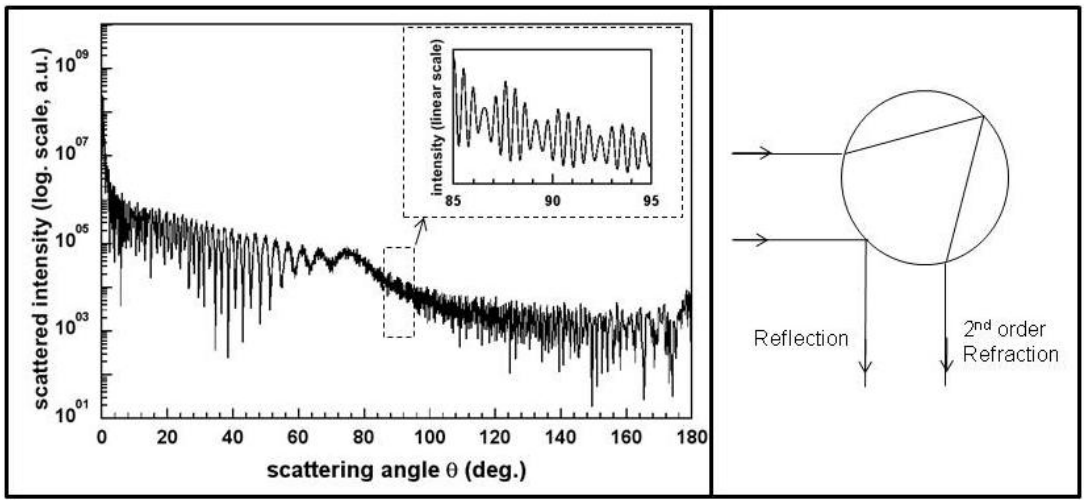

Figure 1: scattering diagram (scattered intensity versus scattering angle) of a 100 µm diameter air bubble immersed in water (relative refractive index of 0.75), computed by LMT. Around 90°, fringes are mainly produced by interferences between reflection and second order refraction.

ILIT combines the advantages of interferometric techniques for the size measurement precision, and imaging techniques for object localization and the ability to isolate different objects from each other. Figure 2, gives a schematic view of ILIT experiments, for a scattering angle θ=90°, a collecting lens of diameter *A* (collection angle α), and the sensor array (CCD of the camera) placed in an out of focus plane distant by d_x from the image plane. The fringes generated by bubbles are projected by the lens on the ccd array where each particle image take a circular shape (the shape of the lens), containing a fringes pattern, depending on the bubble size. The location of the circle is related to the bubble location in the laser sheet, ensuring a separation of different bubble images. Figure 3 gives an example of a droplet spray ILIT image.

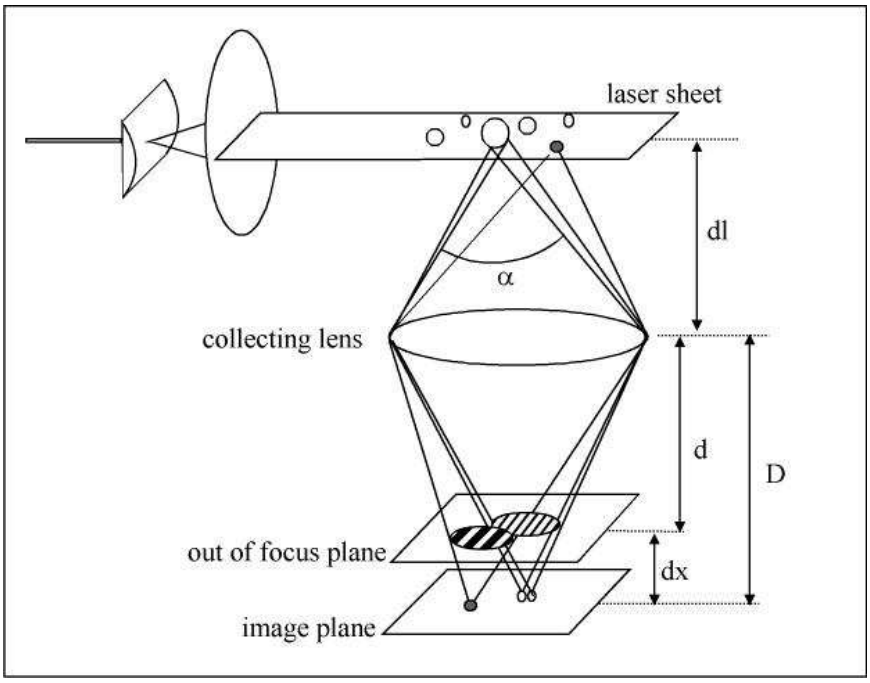

Figure 2: ILIT configuration.

The size of the circle delimiting the particle image only depends on the out of focus degree (distance d_x in figure 2), and the number of fringe in the circular shape depends only on the particle size. The image circle contains the same number of fringes than the lens surface. The lens diameter A and the circle diameter *a* verify

$$a = A\frac{D-d}{D} = A\frac{d_x}{D}$$

If *f* designates the fringes number in the out of focus plane, that is to say $f = N/a$, the fringes angular spacing is then written as

$$\Delta\theta = \frac{\alpha}{N} = \frac{\alpha}{af}$$

Considering a CCD sensor, the number of fringes can be directly evaluated from the size of the circular boundary and the fringes frequency expressed in pixel and pixel^{-1} respectively, by $N = a_p f_p$, leading to

$$\Delta\theta = \frac{\alpha}{a_p f_p}$$

Generally, the diameter of the droplet or the bubble is roughly inversely proportional to the fringes spacing $\Delta\theta$. The bubble diameter d_B is then written as

$$d_B = \kappa \cdot \frac{1}{\Delta\theta} = \frac{\kappa \cdot a_p \cdot f_p}{\alpha}$$

where the coefficient κ can be determined theoretically, by geometrical optics (with some assumptions) or by LMT (assuming a perfect spherical shape).

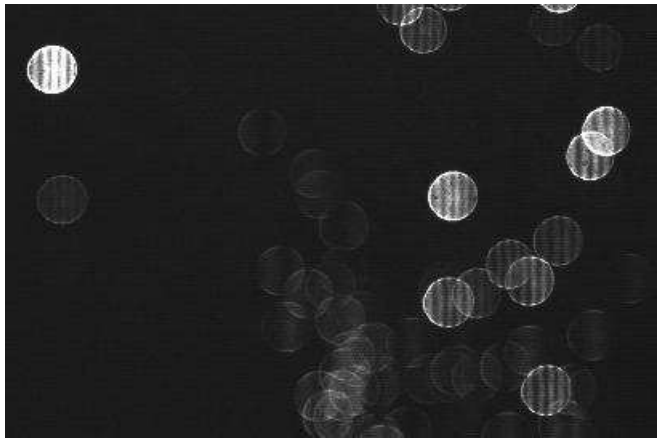

Figure 3: Out of focus images of a droplet spray recorded with a standard 50 mm lens.

The schematic view of figure 2 is not complete. In our experiments, bubbles are immersed in water but the collection optics and the ccd sensor are in air. Then, the collection angle in air α is changes to β in water, as illustrated in figure 4. However, the number of fringes contained in angles α and β are identical and the relation between bubble diameter and the number of recorded fringes becomes

$$d_B = \frac{\kappa_w N}{\beta} = \kappa_w N \frac{n_w}{\alpha} \quad (1)$$

where :

- $\kappa_w(n_{water}, \theta, \lambda)$ is a function of water refractive index n_w, scattering angle θ (90° in our case) and wavelength λ. κ_w is calculated by using an optical scattering model (LMT for us). In our case, $\kappa_w \approx 52 \mu m.\deg$.
- α is the collection angle in air, deduced from a calibration procedure.
- $N = a_p f_p$ is the number of fringes, with the circle radius a_p (in pixel) and the fringes frequency f_p (in Pixel^{-1}) deduced from image processing.

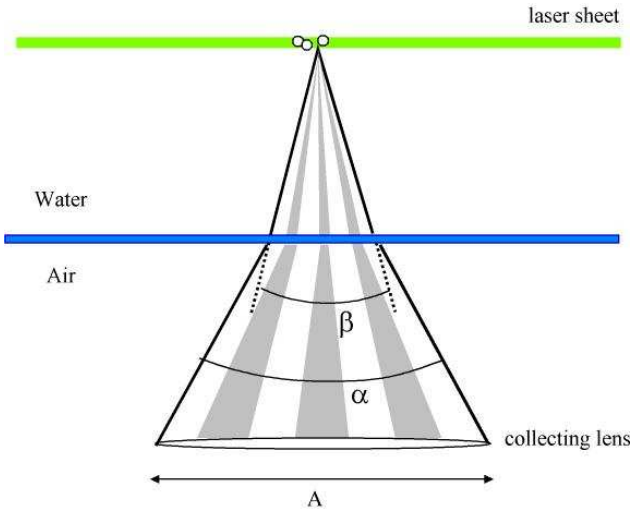

Figure 4: Collection angle change through the tank wall.

BUBBLE SIZE LIMITATIONS AND SPHERICAL ABERRATIONS

The lower limit of ILIT for bubble size measurement is fixed by the lower number of fringes measurable in bubbles images. Assuming that *N=2* fringes is a reasonable limit, from Eq. (1), it can be seen that a large collection angle α is needed to measure small bubbles. Considering the large distance at which the collection optics is set in our application (about *1 m*), large lenses diameters are needed. Figure 5 shows the minimum measurable diameter as a function of the collection angle α. To reach the objective of bubble size measurement lower than 20 µm, a collection angle of about 8° is then needed. Considering a distance of *1m* (equivalent in air) between the bubble flow (laser sheet) and the lens, a lens with effective aperture approaching 200 mm is required, that is to say 10 times the standard lenses aperture.

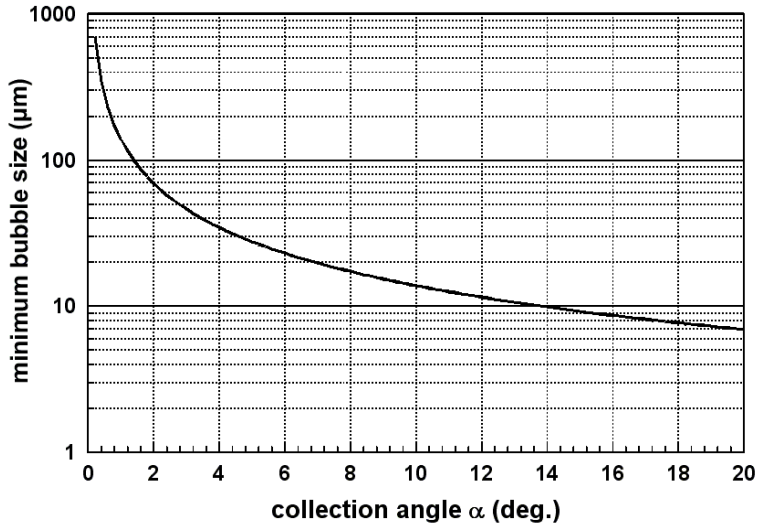

Figure 5: minimum measurable diameter (corresponding to 2 fringes) as a function of the collection angle α.

A large spherical lens (diameter A=200 mm and focal lens f=450 mm) is first consider. Figure 6 shows a schematic view of optical rays, emitted from a single point located in the object plane and refocused by the lens in the image plane to form a point image. The upper part of the figure represents the ideal case of a perfectly stigmatic lens. All rays intersect in a single image point. The lower part of the figure represents rays behavior through a “real” spherical lens. In this case, rays coming from a single point no more intersect in a single image point. The paraxial rays (close to the lens center) intersect in the image plane but edge rays intersect at closer distances. This stigmatism default is well known as spherical aberrations. As a consequence, in the image plane, the point image is no more a single point but a point with some dimensions, surrounded by a halo of light. The effect of spherical aberration on out of focus images (ILIT) is illustrated in figure 6. Out of focus images of a glass fiber are represented for different out of focus plane locations. For very large out of focus (out of focus plane close to the lens), the fiber image shows 8 fringes, only 7 on the second out of focus plane, and so on. When moving the recording plane toward the image plane, the boundary fringes progressively overlap, leading to a dramatic under estimation of the fringes number. Unfortunately, a large out of focus degree it is not reasonable.

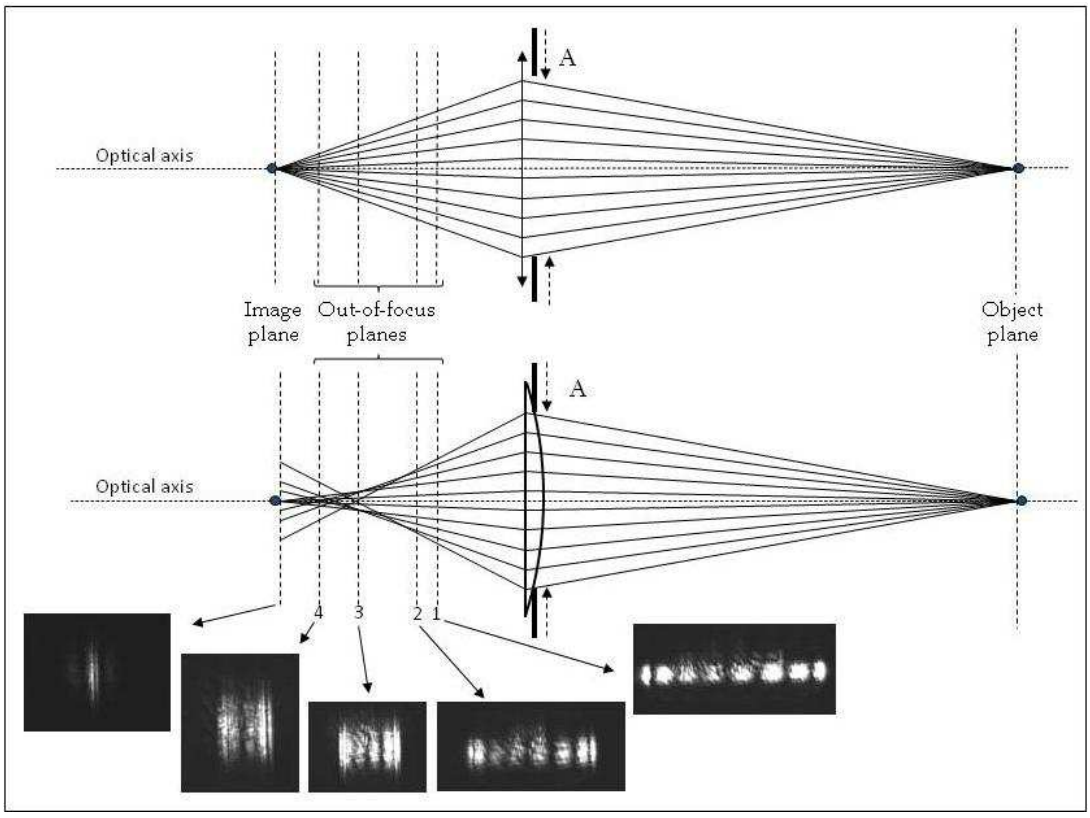

Figure 6: Effect of spherical aberrations on out of focus images.

In case of droplets or bubbles, the out of focus images are full circles and not a line as for the glass fiber. With the larger out of focus degree considered in figure 6 (plane 1), the line length (circle diameter for spherical particles) equal half the full image size, leading to an important (and quasi systematic) overlapping between bubble images, prohibiting the extraction of individual sizes from

fringes frequency. One can deal with some amount of overlapping (depending on the image processing) but in a reasonable limit.

In conclusion, spherical aberrations cannot be eliminated without reducing the lens aperture (increasing the lower measurable size) or without using a very large out of focus, prohibiting simultaneous sizing of several bubbles.

ABERRATION FREE SPECIFIC LENS

Our aim is to perform small nuclei size measurement at large distance by ILIT. The problem to solve is to ensure a large collection angle at large distance while avoiding the negative effects of spherical aberrations. Spherical aberration can be reduced or eliminated by using lenses with non-spherical surfaces. A specific lens assembly has been designed and manufactured to eliminate spherical aberration and to keep a large effective collection angle. One of the lenses has an aspherical profile in order to eliminate spherical aberrations. The optical arrangement consists of two plano-convex lenses in order to reduce the other geometrical aberrations, responsible for distortions of images at the edges of the sensor (departing from the optical axis). The lens assembly has been designed to work at a fixed optical distance (equivalent in air) of *1 m*, allowing measurement through *1 m* in water and a glass window of about *100 mm*. The effective aperture of the optics has been experimentally checked to be 190 mm, as expected. The corresponding minimum bubble diameter (for two fringes) is 12.68 µm. The effect of manufacturing default on the lenses surfaces have been observed on the out of focus images but frequency measurement is not strongly affected. Note that chromatic aberrations have not been considered because the Laser illumination is monochromatic. The design has been done for a given wavelength (λ=532 nm).

EXPERIMENTAL SET-UP AND CALIBRATION

Figure 7 shows the experimental set-up. If we assume the theoretical value of coefficient κ_w and refractive index value of water n_w, the only needed calibration consists in evaluating the effective collection angle α. Generally, ILIT (or ILIDS) measurement are performed using a standard commercial lens. A numerical aperture of the lens is usually specified and the collection angle could be theoretically deduced from it and from the focal length and the working distance. However, the numerical aperture is usually defined for use at infinity (object distance >>focal length) and most of the lens are not completely free from spherical aberration. Returning to figure 3, showing an example of out of focus images recorded at 500 mm with a 50 mm standard lens, with a positive out of focus (camera moves toward the lens), the effect of spherical aberration is visible as the bright circle bordering the circular images. In practice, the effective collection angle is different from the theoretical one and varies with the degree of defocusing. A full calibration procedure is usually recommended for ILIT. But in case of bubble size measurements, this calibration procedure is complicated.

In our case, we first moved backward the ensemble camera/lens from the tunnel, in order to image a calibration target in air. The distance between the target and the lens is fixed at 1 m and the distance between the CCD sensor and the lens is adjusted to focus on the target. A magnification ratio is

deduced. The measured magnification ratio equals 0.465. The magnification ratio predicted from the lens assembly properties (optical design) equals 0.464. Next, the camera is moved forward to focus on the laser sheet (on illuminated bubbles). This procedure ensures that the optical distance between the laser sheet and the lens is 1 m with a precision easily better that 1%. Next, the ccd sensor is moved toward the lens to set the out of focus position (d_x=*3 mm* in our case).

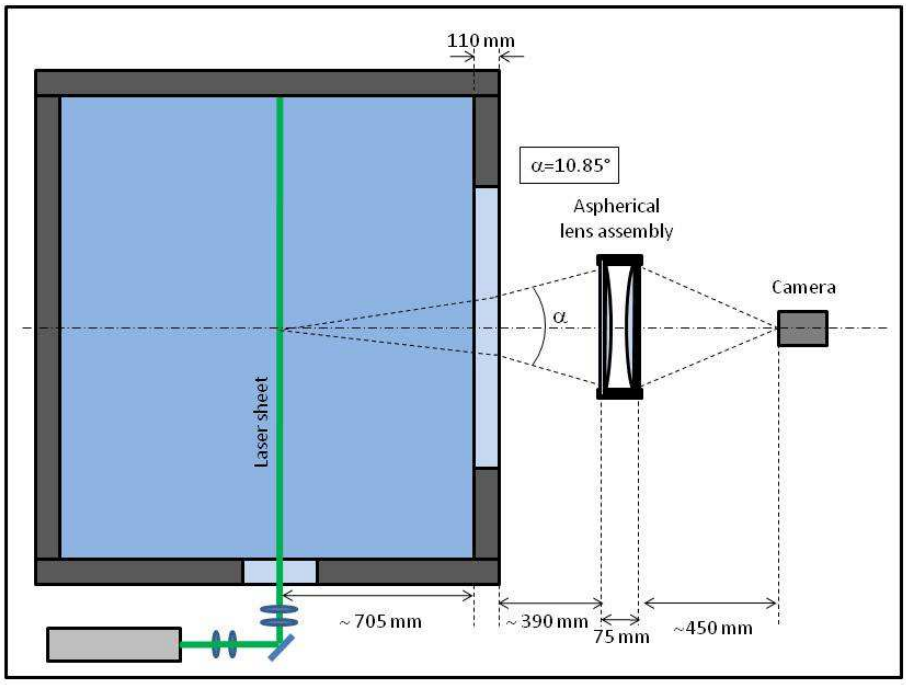

Figure 7: Experimental set-up in cavitation tunnel.

To determine the collection angle α, the effective aperture of the lens assembly must be precisely estimated. The lens diameter is *200 mm* but its manufacture and design guaranty only an effective diameter of 190 mm. A 190 mm aperture (part of the support) is then placed in front of the first lens. The key point was to check the effective aperture of the lens. To do so, apertures (mask) of different sizes (80 and 100 mm) have been placed (in air) in front of the lens. Out of focus images of bubbles illuminated by a very thin laser sheet have been recorded, with the masks and without mask. For a given out of focus, the image circle diameter is theoretically proportional to the aperture diameter. Then the ratios between image circle diameters (in pixel) have been compared to the ratio between physical apertures diameters. This simple procedure would have evidenced if the effective lens aperture was smaller than expected because of spherical aberrations. The lens assembly aperture has been checked to be equal to 190 mm ± 1 mm and the collection angle is then α=10.85°± 0.1°.

The ccd sensor array is a 1600×1200 pixels with square pixels of *7.4µm*. The lens assembly focal length is about *327 mm*, the magnification ratio is 0.465 and the field of view *25.4 mm×19 mm*. The out of focus distance is fixed at *3 mm* toward the lens. The laser sheet is located *1 m* (equivalent in air)

from the lens. The collection angle α is *10.85*°, corresponding to a minimum measurable diameter of about 12.7 µm (2 fringes).

There is also an upper limit for bubble size. It depends not only on the collection angle but also on pixel size and out of focus degree. The greater measurable size corresponds to a number of fringes of about half the image circle diameter. In our configuration, the image circle diameter equals 166 pixels and the corresponding bubble diameter should be greater than 500 µm. However, bigger bubbles have a very bright image and the limited dynamic range of the camera, associated with the necessity of a high laser power to make visible the smaller bubbles, leads to an effective upper limit of about 200 µm.

IMAGE PROCESSING

Figure 8 shows an ILIT image recorded in the tunnel. Two particle images are clearly visible in this image: a bubble image showing horizontal fringes as predicted by the ILIT model and a particle image showing a more irregular pattern. This second image corresponds to a solid particle. ILIT is generally applied to droplets sprays and to droplet size of several hundreds of microns. It is then unusual to face solid particle mixed with the objects of interest. In the present situation, we investigated very small bubbles (down to 10 µm) and solid particles in the same size range are then visible. Fortunately, the horizontal fringes analyzed in ILIT are the consequence of transparency and spherical shape of bubbles. Solid particles produce complex interference pattern, due to their irregular shapes. It is then possible to separate solid particle from bubbles with ILIT by analyzing the fringes pattern of particle images.

The key steps of the image processing we adopted are the following:

1. A background image is subtracted and the image dimension is extended to a 2048×2048 image in order to allow the use of Fast Fourier Transform algorithms.
2. The resulting image is normalized and filtered (see figure 9-a) in order to smooth the fringes, to facilitate the detection of the circular images (step 4).
3. A spatial derivative of the filtered image is computed to extract the boundaries of particle images (figure 9-b).
4. Circles are located by computing a convolution product between the boundary image and a ring whose diameter is defined by the optical configuration parameter (166 pixels in the present case). This step is an iterative process. The first detected particle images are removed from the boundary image which is normalized again and a new convolution product is computed to detect less contrasted particle images. Such an interactive process is needed to detect simultaneously the pale images of the smallest bubbles and the bright images of the biggest. In figure 9-c, the particle images already detected has been subtracted from the boundary image. A third particle image is now clearly visible. it will be detected at the third iteration.

5. The fringes patterns are then analyzed by means of 2D Fourier transforms. Bubble images are validated, on the basis of fringes frequency angle and contrast criterions. In figure 9-d, images 1 and 3 correspond to bubbles whose diameters equal 62.2 µm and 11.2 µm respectively (9.75 and 1.76 fringes). Image 2 corresponds to a solid particle and is not validated.

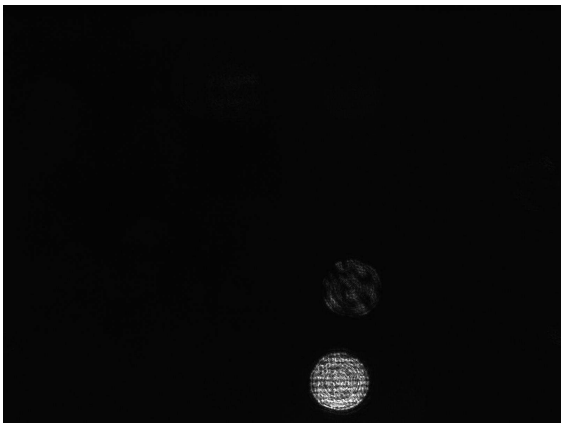

Figure 8: ILIT recorded image.

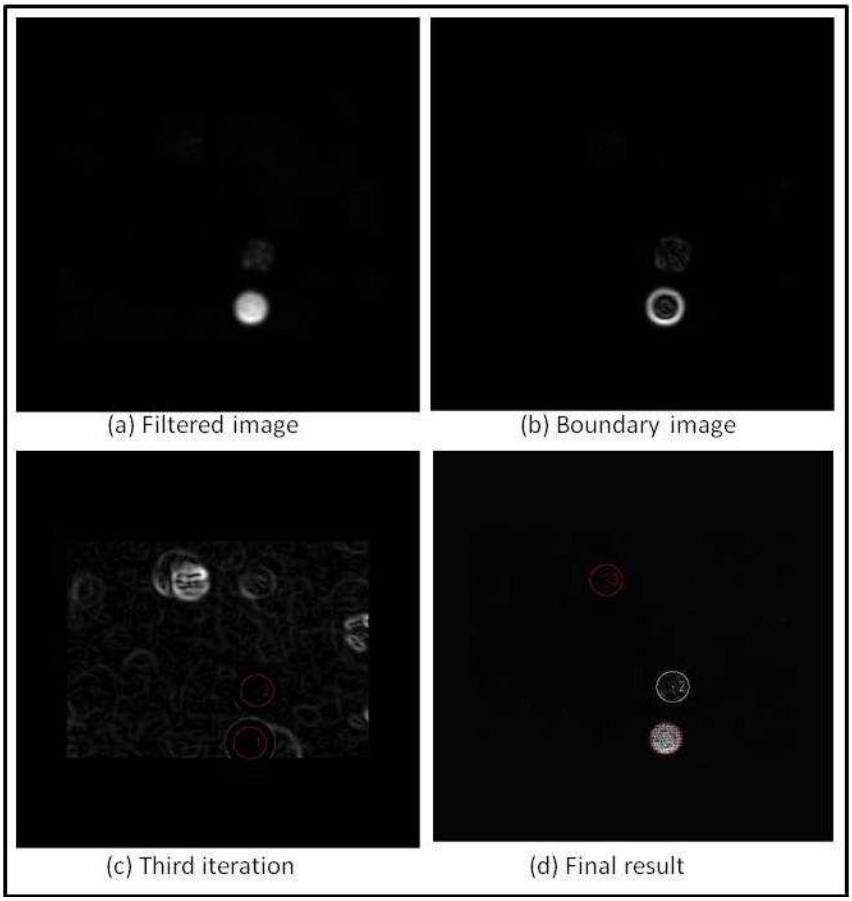

Figure 9: key steps of the image processing.

Note that the image circle size actually varies by a few pixels from one bubble to another. This variation will be discussed later in the paper but the real size of the image circle is measured before

the fringes frequency analysis, to accurately determine the fringes number and bubble diameter. Finally, note that about 1 hour is needed to process 100 images on a laptop.

RESULTS AND DISCUSSION

The French large cavitation tunnel has 2 test sections. Measurements presented below have been done in the large test section (*2 m x 1,35 m*). The ILIT set-up is the one illustrated in figure 7. 2000 images have been recorded for 4 different pressure conditions in the tunnel (207, 567, 927 and 1287 mbar). Figure 10 shows the size distribution obtained by ILIT for these 4 conditions. No bubble smaller than 10 µm are considered, because the corresponding number of fringes would be less than 1.57. For such a small number of fringes it is not possible to distinguish solid particle images from bubble images. Results are organized in terms of particle size ranges 5 µm wide. Note that the number of validated bubbles with respect to the total number of particle images detected (solid particles + bubbles) is in the order of 5%.

Until now, nuclei content of the cavitation tunnel was measured only by means of the Centerbody Susceptibility Meter (CSM) [8]. The CSM provides bubble cumulative distributions which are the only reference we have to compare our ILIT results. Moreover the CSM provides cumulative distribution in concentration units (number of nuclei per cm^3). To express our results in terms of concentration, the measurement volume must be estimated.

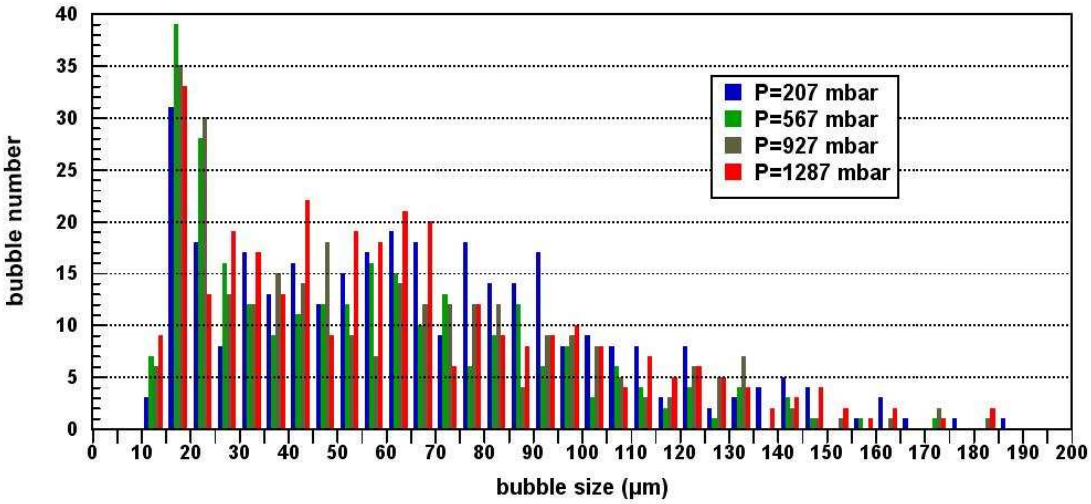

Figure 10: Bubble size distribution in the cavitation tunnel measured by ILIT.

CONCENTRATION MEASUREMENT

It is well known that techniques based on laser sheet illumination are not suitable for concentration measurements. In such techniques, the measurement volume must be estimated from the field of view and the laser sheet width. But a laser sheet generally shows a Gaussian profile and the exact limit of the measurement volume is very hard to define. Moreover, the intensity of light scattered by particles strongly depends on the particle size. As a consequence, the measurement volume should vary with particle size (increasing with particle diameter). Figure 11 shows the laser sheet profile as it

has been measured after the measurement campaign. A rough evaluation of the measurement volume can be deduced from the profile width and from the field of view but we have to assume a threshold value under which the bubble image will be not bright enough to be detected. In other words we have to chose an arbitrary value for this threshold.

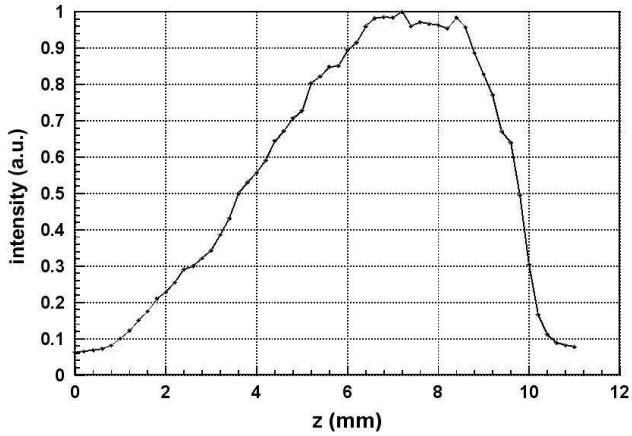

Figure 11: Measured Laser sheet profile.

However, ILIT can offer an alternative way to determine the depth of the measurement volume (depending on the optical parameters used). Indeed, the circle size of the bubble image depends on the out of focus degree. It then depends on the distance between the bubble and the lens as illustrated in figure 12. Any displacement Δz of the object distance d_l is associated to a displacement of the image distance D and to a modification of the out of focus image diameter d_c following

$$\Delta d_c = -\frac{A}{d_l}\frac{M^2}{n_w}\Delta z$$

where A is the lens aperture, n_w is the refractive index of water and where the circle diameter d_c is expressed in mm (as object distance d_l). The circle diameter variation with the displacement Δz can be calculated directly in pixel per mm, leading to *9.3 pixel.mm*$^{-1}$. Inversely, one pixel variation in the circle diameter is associated with a displacement of the bubble in z direction

$$\gamma = \frac{\Delta z}{\Delta d_c} \approx 108\ \mu m.pixel^{-1}$$

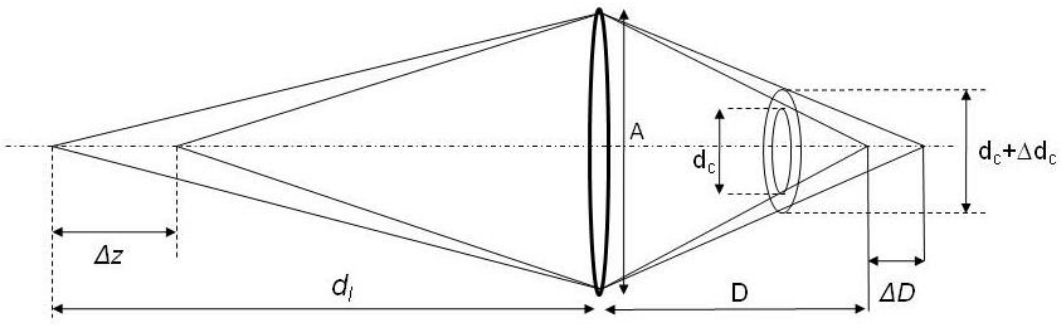

Figure 12: Variation of the circle diameter with *z* coordinate of the bubble.

Some variations with respect to the 166 theoretical values are visible in images and the real size of any image can be extracted. But these variations are not only due to the z coordinate of the bubble. Indeed, these circle diameter variations are also due, for a part, to the non spherical geometrical aberrations. Bubbles located at the edges of the imaged field have weakly distorted images. The image is no more bounded by a perfect circle but by an oval shape. An average circle diameter can be however defined and a correction to the measured diameter is applied as a function of the bubble position. After applying this correction, average circle diameter and standard deviation have been computed for each particle size range. Figure 13 displays the standard deviation of the image circle diameter computed for each bubble size range (20 µm wide), on the results presented figure 10 (all the 4 cases together). A quasi linear evolution of the standard deviation can be extracted from figure 13. Deviation from this tendency for greater bubble is due to the small number of bubble constituting the sample in these size ranges. The standard deviation $\sigma(d_B)$ in image circle diameter can be easily associated to a measurement volume, function of the bubble diameter d_B,

$$V(d_B) = 2 \times \sigma(d_B) \times \gamma \times S$$

where $S \approx 485\ mm^2$, the field of view area.

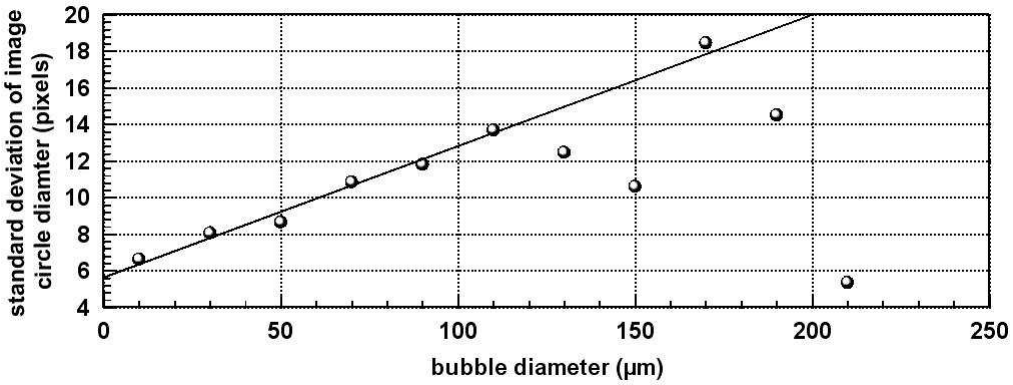

Figure 13: Standard deviation of the image circle diameter as a function of the bubble diameter.

The variable measurement volume is then used to convert the results of figure 10 in terms of bubble concentration. Figure 14 displays the cumulative bubble size distribution expressed in bubble number per cm^3, for the 4 pressure conditions. Bubble concentrations are in the same order of those measured by CSM in conditions closed to ours and presented in figure 15.

CONCLUSION

A specific ILIT arrangement, dedicated to nuclei content characterization has been developed. This technique can be used directly in the tunnel test section to provide a direct control of the nuclei content during cavitation tests. In addition to bubble size distribution, bubble concentration can be evaluated from statistic on ILIT results. Results are compatible with those of CSM, the reference technique used in the French Cavitation Tunnel.

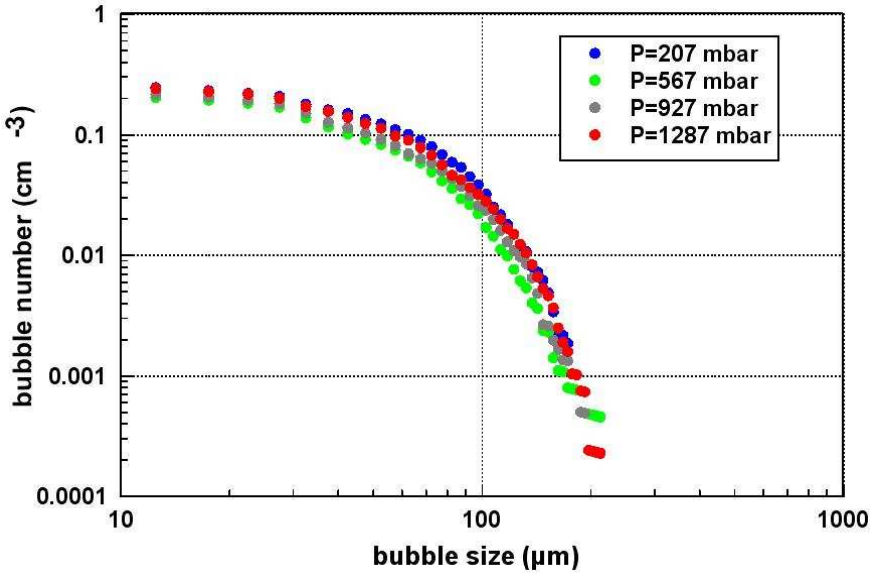

Figure 14: Cumulative distribution of bubble in the cavitation tunnel test section.

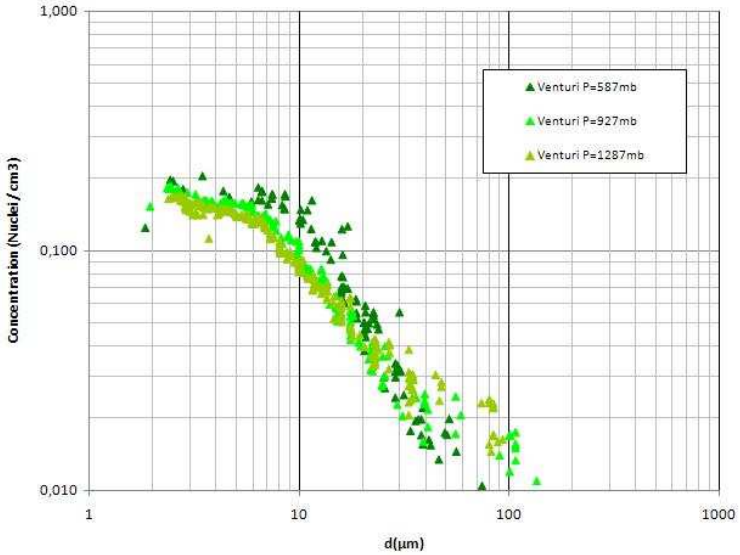

Figure 15: Cumulative nuclei distribution obtained by CSM measurements in similar conditions.

REFERENCES

1. Gindroz B & Billet M.L., 1993, “Influence of the nuclei on the cavitation inception for different types of cavitation on ship propellers”, ASME FED – Vol.177, New Orleans, USA.
2. Billet M.L., Wilson M.B., Bailo G.M., Gindroz B, Lee J.T, Bark G., Friesh J., Hoshino T, Szantyr J.A., “Report of the Cavitation Committee”, Proceedings of the 21st ITTC, Tronheim, Norway,Vol. 1, 1996, pp. 63-126.
3. Lecoffre Y, Chantrel P. & Tellier J., "Le Grand Tunnel Hydrodynamique (GTH)", ASME Winter Annual Meeting, Boston, USA, December 1987.
4. Fréchou D., Dugué C., Briançon-Marjollet L., Fournier P., Darquier M. , Descotte L., Merle L., “Marine Propulsor noise investigation in the hydroacoustic water tunnel GTH ”, 23rd Symposium on Naval Hydrodynamics, September 2000, France.
5. Ragucci R., Cavaliere A., Massoli P., “Drop sizing by Laser light Scaterring Exploiting Intensity Angular oscillation in Mie Regime”, Part. Syst. Charact. 7, 1990, pp. 221-225.

6. Glover A.R., Skippon S.M. and Boyle R.D.. “Interferometric Laser imaging for droplet sizing: a method for droplet-size measurement in sparse spray systems”, Appl. Opt. 34 , 1995, pp. 8409-8421.
7. Pu S., “Development of interferometric methods for particle fields characterisation”, Phd thesis, October 2005, Université de Rouen, France.
8. Pham T, Michel J-M, Lecoffre Y., “A new design of the Cavitation Susceptibility Meter”, Conference on cavitation, 1993, Birmingham, UK.